On the mechanism of deep craters formation under the action of high power ytterbium-fiber laser

E A Kochurin[1], V V Lisenkov[1,2], V V Osipov[1], V V Platonov[1] and N M Zubarev[1,3]

[1] Institute of Electrophysics of the Ural Branch of the Russian Academy of Sciences, Amundsen 106, Ekaterinburg 620016, Russia
[2] Ural Federal University, Lenina Avenue 51, Ekaterinburg 620000, Russia
[3] Lebedev Physical Institute of the Russian Academy of Sciences, Leninsky Avenue 53, Moscow 119991, Russia

E-mail: kochurin@iep.uran.ru

Abstract. Stability of a liquid crater wall formed under the action of an ytterbium-fiber laser in the course of the Nd^{3+}:Y_2O_3 nanopowder production is studied theoretically. It has been shown that hydrodynamic instability can develop on the melt-vapor interface as a result of the tangential discontinuity of the velocity between the vapor stream and molten crater wall. The characteristic spatial and temporal scales are estimated in the framework of the proposed qualitative model, they are found to be 20–90 μm and 20–50 μs, respectively, that is in good agreement with experimental data. Thus, the droplet formation time (during which the amplitude of the boundary perturbation reaches the wavelength order) is much smaller than a pulse duration of the ytterbium-fiber laser (1360 μs). This means that a significant amount of material can be removed from the crater due to formation of microscale droplets during the irradiation. This mechanism can explain the much greater crater depth for the fiber laser than for CO_2 laser (a pulse duration for which is 370 μs).

1. Introduction

The radiation impact of CO_2 laser ($\lambda = 10.6$ μm) and ytterbium-fiber laser ($\lambda = 1.07$ μm) pulses on the Nd^{3+}:Y_2O_3 targets in the course of nanopowder production is theoretically and experimentally investigated in [1,2]. The nanopowder was created in the flow of near atmospheric pressure air. The interest for using the fiber laser is caused by its higher efficiency (up to 30%) with respect to CO_2 laser. The experiments show that the radiation of fiber laser leads to formation of significantly deeper craters on the target surface than for the pulsed CO_2 laser (figure 1). Wherein, the total energy of a pulse for two lasers was almost equal and was about 1 J. The needle-shaped profile was formed on the target surface under the action of the fiber laser radiation, see figure 1b. As a result the efficiency of the process decreased in consequence of reducing the radiation absorption coefficient. It is also noted in [2] that this effect can be minimized by means of increasing the velocity of beam shift along the target surface and diameter of laser spot.

The process of melt displacement from the crater formed under the pressure of target vapor is studied for repetitively pulsed CO_2 laser in detail in [3]. It should be noted that the initial stages of the crater formation for both types of the lasers are qualitatively the same. Under

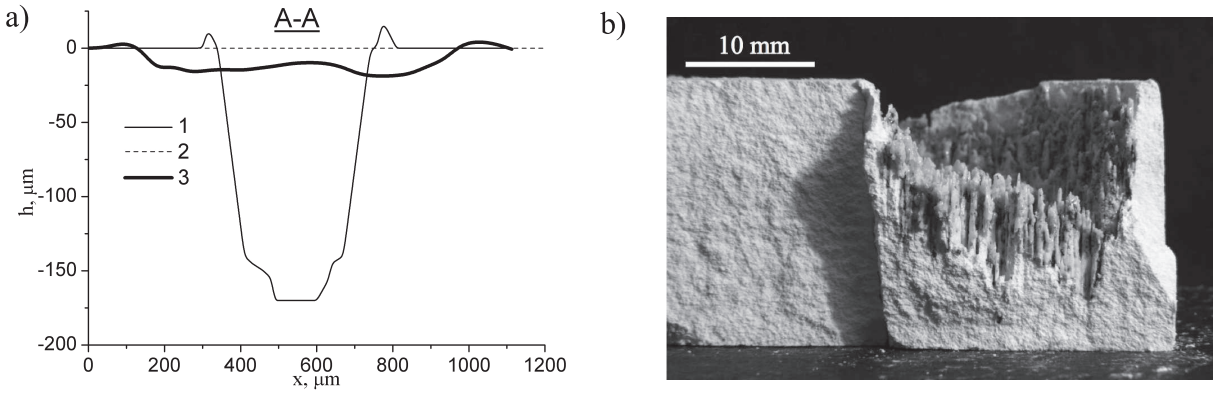

Figure 1. (a) Profiles of the craters for the target with 1 mol% of Nd^{3+}:Y_2O_3: 1—under laser irradiation using a fiber laser with an output power of 700 W, pulse duration 1.36 ms and a pulse energy of 0.95 J; 2—level of the target surface; 3—profile for LAERT CO_2 laser with a peak power of 5.8 kW and a pulse energy of 0.93 J. (b) Profile of a target surface after irradiation using the fiber laser [1, 2].

the action of excess vapor pressure a rib on the target surface arises and becomes visible at an exposure time of about 100 μs. Further, a process of deepening of the crater takes place due to both the evaporation and displacement of melt. In particular, occurrence of deep craters for the fiber laser can be explained by the presence of inhomogeneities in the material Nd^{3+}:Y_2O_3, which can lead to mechanical destruction of the surface [1, 2]. However, a mechanism of deep melting of the targets under the action of ytterbium-fiber laser radiation remains not entirely clear; the depth of the craters differs almost by an order, see figure 1a.

The work [4] is devoted to investigation of the impact of an ytterbium-fiber laser radiation on the dielectric targets YSZ, ZnO, YAG. It was shown that for all types of the materials the deep craters are formed. Authors associate this effect with the so-called spike-like melting [5], which can be observed when the depth of the crater is from 10 to 50 times larger than its diameter. This mechanism of melting takes a place when, starting from a certain radiation intensity, the reactive pressure of material vapor heavily deforms the melt surface forming almost vertical wall of the crater. The property of deep melting of materials under the action of the fiber laser irradiation is widely used in metal cutting, for example, it is demonstrated in [6] that an ytterbium-fiber laser provides the cutting of alloyed steel sheets with a thickness of 4 mm at a rate that is four times greater than the rate provided by the CO_2 laser of the same power.

It should be noted that the process of the crater formation under the action of a pressure gradient is characteristic for many physical phenomena, such as vacuum arc functioning [7], electron or ion irradiation on targets [8, 9]. Wherein, the development of various types of hydrodynamic instabilities (Rayleigh–Taylor, Meshkov–Richtmayer, Plateau–Rayleigh and Kelvin–Helmholtz) can occur during these processes. A possibility of the instabilities development under the action of a pulsed high power laser is considered in [10]. For the laser synthesis of nanopowders the hydrodynamic instabilities in a laser plume crater can be considered as an undesirable effect, since in the process of their development spherical droplets of relatively large scale (1–100 μm) can be formed. The required nanoscale particles can be formed only as a result of condensation of the material vapor. The distribution function of the micro-drops with respect to size is shown in figure 2 obtained in [11]. It can be seen that the largest number of particles has a scale from 20 μm to 100 μm. Thus, the deep crater formation under the action of the fiber laser is accompanied by massive emission of the target material in the form of liquid microscale droplets. It is natural to assume that an occurrence of these particles is related with

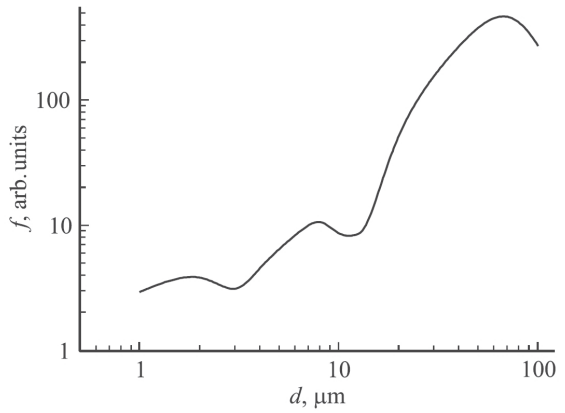

Figure 2. Distribution function of the drops with respect to size [11].

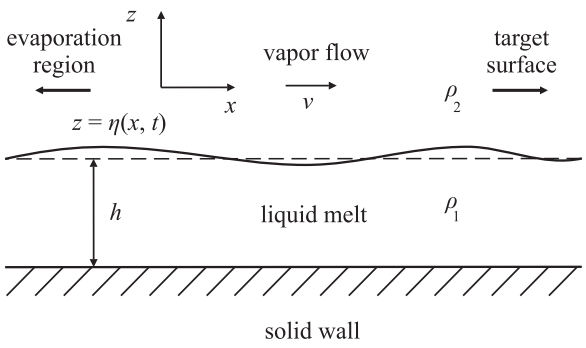

Figure 3. Scheme of the model geometry.

the development of hydrodynamic instabilities in the laser plume crater. In the present work we theoretically investigate the stability of melted crater wall and show that its surface becomes unstable at the scale of 20–90 μm.

2. The model description

The process of droplets formation is nonlinear physical phenomenon occurring in 3D-geometry and its direct analytical description is an extremely complicated problem. So, it is relevant to propose a model qualitative describing the process of the instability development and allowing to estimate the characteristic scales of the droplets size and time of their formation. Since, the diameter of the crater (200–400 μm) is high relatively to the size of microdroplets (1–100 μm), we assume the problem to be plan symmetric, i.e. the geometry under consideration is equivalent to scheme shown in figure 3. As it was mentioned earlier the excess vapor pressure heavily deforms the melt surface. Under the action of reactive pressure the liquid melt moves from evaporation region towards the crater walls. It is noted in [12, 13] that an additional factor of the melt displacement is termocapillary convection arising as a result of inhomogeneous distribution of temperature on the bottom (evaporation region) and colder crater walls. Thus, we study the stability of vertical melted wall of the crater.

The melt occupies the region with subscript "1" and vapor flow does "2" that. Also for the simplicity of description we assume the motion of the melt and vapor to be incompressible and potential (undissipative). Thus, the velocity potentials satisfy the Laplace equatons

$$\nabla^2\Phi_1 = 0, \quad z < \eta(x,t), \quad \nabla^2\Phi_2 = 0, \quad z > \eta(x,t), \tag{1}$$

where $z = \eta(x,t)$ defines the shape of the boundary (in unperturbed state $z = 0$). The kinematic and dynamic boundary conditions at the interface have the following form:

$$\frac{\partial\eta}{\partial t} = \frac{\partial\Phi_1}{\partial z} - \frac{\partial\Phi_1}{\partial x}\frac{\partial\eta}{\partial x}, \quad z = \eta(x,t), \tag{2}$$

$$\rho_1\left(\frac{\partial\Phi_1}{\partial t} + \frac{(\nabla\Phi_1)^2}{2}\right) - \rho_2\left(\frac{\partial\Phi_2}{\partial t} + \frac{(\nabla\Phi_2)^2}{2}\right) = \sigma\frac{\partial^2\eta}{\partial x^2} + P_0, \quad z = \eta(x,t), \tag{3}$$

where ρ_1 and ρ_2 are the mass densities of the melt and vapor, respectively, σ is the surface tension coefficient, P_0 is the Bernoulli constant defined by the boundary conditions. At the interface the velocity potentials obey the condition

$$\partial_n\Phi_1 = \partial_n\Phi_2, \quad z = \eta(x,t), \tag{4}$$

where $\partial_n f = (f_z - f_x\eta_x)/\sqrt{(1+\eta_x^2)}$ denotes the derivative along the normal to the surface. Let us write the boundary conditions far from the interface

$$\Phi_1 = 0, \quad z = -h, \quad \Phi_2 = vx, \quad z \to +\infty, \tag{5}$$

where h is the thickness of the melt layer (we assume that it is a constant), v is the velocity of vapor flow, which is close to the sound speed. The concluding equation is the condition at the bottom

$$\frac{\partial \Phi_1}{\partial z} = 0, \quad z = -h. \tag{6}$$

This equations system describes the motion of two ideal incompressible fluids (melted crater wall and flow of vapor) with the interface under the action of destabilizing shear stress and surface tension, which aims to provide the stability of the boundary. As it easy to see, the system involves the nonlinear differential equations (2) and (3), so its full analytical description is complicated. In the present work we consider only linear stages of instability development, i.e. the surface perturbations are infinitesimal. The nonlinear evolution of Kelvin–Helmholtz instability is studied in [14, 15].

3. The linear stability analysis

The system of the equations of motion (1)–(6) has an exact analytical solution: $\eta = 0$, $\Phi = 0$, $\Phi_2 = vx$, which allows finding the Bernoulli constant $P_0 = -\rho_2 v^2/2$. Let us introduce the perturbed velocity potentials $\phi_1 = \Phi_1$, $\phi_2 = \Phi_2 - vx$ and rewrite restricted by linear approximation the equations (2), (3) and (4) in terms of the new variables,

$$\frac{\partial \eta}{\partial t} = \frac{\partial \phi_1}{\partial z}, \quad \rho_1 \frac{\partial \phi_1}{\partial t} - \rho_2 \frac{\partial \phi_2}{\partial t} - \rho_2 v \frac{\partial \phi_2}{\partial x} = \sigma \frac{\partial^2 \eta}{\partial x^2}, \quad \frac{\partial \phi_1}{\partial z} = \frac{\partial \phi_2}{\partial x} - v\frac{\partial \eta}{\partial x}.$$

It is easy to obtain [16] the dispersion relation for linear waves on the surface $\eta \sim \exp(\mathrm{i}kx - \mathrm{i}\omega t)$

$$\rho_1 \omega^2 = \tanh(kh)\left(\sigma k^3 - \rho_2(\omega - vk)^2\right), \tag{7}$$

where ω is the frequency, k is the wave number. In deriving of (7) we took into account that $\rho_2 \ll \rho_1$. The relation (7) can be solved relatively ω

$$\omega = \frac{\rho_2 vk \tanh hk}{\rho_1} \pm \sqrt{\frac{\tanh hk}{\rho_1}}\sqrt{(\sigma k^3 - \rho_2 v^2 k^2)}.$$

Thus, the stability of the boundary depends on a sign of the expression $(\sigma k^3 - \rho_2 v^2 k^2)$, for the negative values the instability takes a place and the imaginary part of ω is its increment $\delta = \mathrm{Im}\,\omega$. The interface is stable if $\delta = 0$. As it is easy to see, this condition is satisfied for the perturbations of the following scale

$$\lambda_c = \frac{2\pi\sigma}{\rho_2 v^2}. \tag{8}$$

Because the quantities in the right-hand side of (8) are difficult to be determined with high accuracy, we have taken their values in sufficiently wide range, see table 1 (the estimate for σ is received from [17], the density and velocity of the vapor flow are obtained from experimental data, in particular [18]). As the table shows the characteristic scale of the instability development (the size of droplets formed) is in the range from 20 μm to 90 μm, that is in good agreement with the experimental data (see figure 2).

Table 1. The characteristic values of the parameters of the problem.

σ (N/m)	ρ_2 (kg/m^3)	v (m/s)	λ_c (μm)
0.5–1.5	1.8–2.2	220–300	20–90

From the dispersion relation (7) we can find a maximum instability growth rate, i.e. the time during which the amplitude of the boundary perturbation reaches the wavelength order

$$\tau = \frac{2\pi}{\delta_{\max}} \approx \frac{3\sqrt{3}\pi\sigma}{\rho_2 v^3}\sqrt{\frac{\rho_1}{\rho_2}}, \tag{9}$$

where we took into account that the depth of melt layer is close to size of microparticles formed, i.e. $\tanh(2\pi h/\lambda_c) \approx 1$. The time of the droplet formation estimated from (9) is $\tau \approx 20$–50 μs (the melt density $\rho_1 \sim 4 \times 10^3$ kg/m^3). Thus, the time of droplet formation is smaller than a pulse duration of the CO_2 laser (370 μs) and much less than the fiber laser one (1 360 μs). This means that, in the course of the fiber laser irradiation, the microscale particles are formed in much larger quantities than for pulsed laser, namely due to this mechanism the deep craters on the surface of Nd^{3+}:Y_2O_3 targets can occur. It is worth noting the works [19] and [20], in which the authors investigate the process of metal cutting under the action of powerful laser radiation and shear stress exerted by sharply focused gas jet. Apparently, the mechanism proposed is similar to one studied in [19, 20] except that the role of external gas is played by the vapor flow of target material.

4. Conclusion

A model of the microdroplets formation on the vertical molten crater walls, formed under the action of powerful fiber laser radiation, is proposed in the present work. Theoretical analysis has shown that the interface can be unstable at the scale of 20–90 μm, as a result of tangential velocity jump between the rising vapor flow and liquid crater walls. The characteristic time of the droplet formation is estimated, according to calculations, it does not exceed 50 μs. The experiment shows that the first liquid drops fly out from the target surface at 200–300 μs after appearance of laser plume. Apparently, such delay is related with formation of a sufficient amount of liquid melt required for realization of hydrodynamic instability. Due to the mechanism of thermal conductivity the volume of molten material for the pulsed CO_2 laser is considerably smaller than for the fiber laser because the heat does not penetrate at a large depth during its pulse. Thus, a pulse energy for continuous fiber laser and repetitively pulsed CO_2 laser is almost equal each other, the durations of that are very different, so significantly more microparticles can be formed under the impact of the first one, as it is experimentally observed in the form of deeper craters.

Acknowledgments

The work was supported by the Russian Foundation for Basic Research (projects No. 16-38-60002 and 14-08-00181), the Presidium of the Ural Branch of the Russian Academy of Sciences (project No. 15-17-2-19) and Presidential Programs of Grants in Science (project No. SP-132.2016.1).

References

[1] Osipov V V *et al* 2014 *Tech. Phys.* **59** 716
[2] Osipov V V *et al* 2014 *Tech. Phys.* **59** 724
[3] Osipov V V *et al* 2011 *Tech. Phys. Lett.* **37** 49

[4] Kotov Yu A *et al* 2011 *Tech. Phys.* **56** 652
[5] Bunkin F V and Tribel'skii M I 1980 *Sov. Phys. Usp.* **23** 105
[6] Leibinger P 2010 *Stahlmarkt* **60** 40
[7] Mesyats G A and Zubarev N M 2015 *J. App. Phys.* **117** 043302
[8] Boiko V I *et al* 1999 *Phys. Usp.* **42** 1139
[9] Volkov N B *et al* 2006 *Tech. Phys. Lett.* **32** 424
[10] Brailovsky A B *et al* 1995 *Appl. Phys.* A **61** 81
[11] Lisenkov V V *et al* 2013 *Tech. Phys.* **58** 1469
[12] Seidgazov R D 2009 *J. Phys. D: Appl. Phys.* **42** 175501
[13] Seidgazov R D 2011 *Math. Model. Comput. Simul.* **3**(2) 234
[14] Zubarev N M and Kuznetsov E A 2014 *J. Exp. Theor. Phys.* **119** 169
[15] Moore D W 1979 *Proc. R. Soc. London, Ser.* A **365** 105
[16] Landau L D and Lifshitz E M 1989 *Fluid Mechanics* (*Course of Theoretical Physics* vol 6) (Oxford: Butterworth-Heinemann)
[17] Balakrishnan A *et al* 2010 *Acta Mater.* **58** 802
[18] Osipov V V *et al* 2005 *Quant. Electron.* **35** 633
[19] Johnson R L and O'Keefet J D 1974 *AIAA J.* **12** 1106
[20] Schuocker D *et al* 2012 *Phys. Procedia* **39** 179